Pergamon

Journal of Structural Geology, Vol. 17, No. 10, pp. 1361 to 1373, 1995

0191-8141/95 $9.50+0.00

0191-8141(95)00027-5

Interfering folds in constrictional deformation

S. K. GHOSH, D. KHAN and SUDIPTA SENGUPTA

Department of Geological Sciences, Jadavpur University, Calcutta 700 032, India

(*Received* 3 *July* 1994; *accepted in revised form* 17 *February* 1995)

Abstract—Experiments on buckle folding indicate that in pure constriction ($\lambda_2 = \lambda_3 < 1$) a dome-and-basin pattern develops in initial stages. The domes and basins do not occur along distinct rows, and with progressive deformation they do not evolve into tubular or sheath folds. The pattern is progressively replaced by diversly oriented folds with curved hinge lines. In general constriction ($1 > \lambda_2 > \lambda_3$), there is an association of domes and basins with nonplane noncylindrical folds. The areas of domes and basins are reduced with increasing deformation. There is a dominant fold trend perpendicular to λ_3 with a less dominant trend perpendicular to λ_2. Folds at an angle to these two sets may also occur. The divergent folds link up in smooth arcs or join up at a dome or a basin. Over a relatively large domain the interference pattern produced by general constriction can be recognized by the association of domes and basins with nonplane noncylindrical folds, by occurrence of hair pin bends of hinge lines of open folds, by occurrence of amoeboid outcrop patterns and by absence of a consistent overprinting relation among different sets of folds. Layers subparallel to the λ_1 axis of general constriction may give rise to two or more sets of coaxial cylindrical folds with orthogonal axial surfaces.

INTRODUCTION

A single phase constrictional deformation may give rise to a complex pattern of nonplane or noncylindrical folds (Ramberg 1959, Flinn 1962, Turner & Weiss 1963, p. 509, Ramsay 1967, p. 113, Hobbs *et al.*, 1976, p. 284, Treagus & Treagus 1981, Ramsay & Huber 1983, p. 66, Ramsay & Huber 1987, p. 475, Ghosh 1993, p. 328). Surprisingly, and in contrast with this general notion, there are very few geometrical analyses of naturally occurring fold interference by constrictional deformation, either in the mesoscopic or in the macroscopic scale. This is partly because of the absence of a set of clear-cut criteria by which interfering folds produced in constrictional deformation can be distinguished from those produced by superposed deformations.

Weiss (1959) and Turner & Weiss (1963, pp. 508–509, fig. 14-4) have considered the hypothetical case of synchronous development of two sets of *plane folds* by tangential shortening of layers in two mutually perpendicular directions, with the axial planes of the folds at a right angle to each other. Ramsay & Huber (1983, p. 66 fig. 4.11 E; 1987 p. 475) on the other hand, pointed out that the interference pattern in constrictional deformation should show diverse trends of folds and that the folds should have a less systematic interference geometry than in the case of superposed folds.

Interfering folds by layer-parallel constriction have been produced experimentally by Ghosh & Ramberg (1968). The pattern shows a close association of irregular domes and basins with diversely oriented folds showing arcuations and bifurcations of the fold hinges. Buckling folds were also produced in zones of local constriction in some of the centrifuged models of Ramberg (1966, p. 31 figs. 29, 40, 44 and 45), with two gravitationally unstable layer-systems in which the buoyant source layer rose up to produce domes. A local constrictional deformation was produced by a convergent flow in the source layer. Buckle folding took place in thin competent layers occurring within the source layers. As the domes rose, the competent layers surrounding them became subparallel to the vertical trunk portion of the dome. The resulting folds had diversely oriented axial surfaces (Fig. 1) radiating outward from the domal region and with steeply plunging fold axes.

Treagus & Treagus (1981) made a detailed theoretical analysis of folding in layers oblique to the principal planes of a weakly constrictional deformation. They predicted that under a slight constrictional strain en-echelon periclines will form and that the axes of the folds will show a strong variation in orientation.

There are very few geometrical analyses of naturally occurring fold interference produced by constrictional deformation. The late folds on the cleavage surface in some terrains occasionally show a dome-and-basin structure or an association of domes and basins with strongly arcuate curvilinear folds which cannot be explained by multiple deformations. Thus, for example, the pattern of mesoscopic domes and basins in Fig. 2(a)

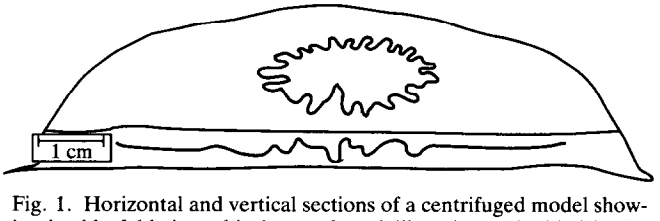

Fig. 1. Horizontal and vertical sections of a centrifuged model showing buckle folds in a thin layer of modelling clay embedded in the source layer of silicone putty. Sketched from fig. 2.9 of Ramberg (1966).

is quite distinct from the pattern produced by superposed buckling (cf. Ghosh *et al.* 1992, figs. 2 and 3). From both experiments and field observations it is known that folding of the axial surface of an early fold by superposed buckling can take place only if the early fold is tight. The occurrence of hair pin bends of the hinge lines and axial surfaces of the open fold in Fig. 2(c) and its close association with domes and basins cannot be explained by superposed folding; the structure is likely to have been produced by a constrictional deformation. Similar structures have been described by Ghosh & Sengupta (1985) from the Kolar Schist Belt of South India. Some of the complex interference patterns from Söröy in Norway were interpreted by Ramsay & Sturt (1973a,b) as a product of constrictional deformation. Treagus & Treagus (1981) suggested that areas with strong plunge variations and with aberrant relationships of folds and cleavages might have undergone a slightly constrictional strain. It was suggested that the model proposed by Treagus & Treagus could explain the structure in the Galloway region of SW Scotland (Stringer & Treagus 1980). According to Turner & Weiss (1963, pp. 508–509) the fold system in the Dalradian Schist of Argyllshire as reported by Roberts (1959) might provide a natural example of fold interference under bulk constriction. Nevertheless, natural examples of folding by constrictional deformation are few in number and their distinctive morphological characteristics are not well-defined in most cases.

The present study is essentially concerned with experiments on buckle folding in layers which undergo simultaneous shortening in two directions. The models were deformed by both *pure constriction* with $\lambda_2 = \lambda_3 < 1$) and *general constriction* (with $1 > \lambda_2 > \lambda_3$). The major objective of this series of experiments is to find out the characteristic geometrical features of the fold interference produced by constrictional deformation, to distinguish between interfering fold morphologies produced in pure and general constrictions and to explore the possibility of determining a set of criteria by which the interference geometry can be distinguished from that produced by multiple deformations.

EXPERIMENTAL METHODS

The machine used for constrictional deformation is an electrically operated twin motor machine. Each of the motors drives in a horizontal direction a set of two oppositely facing vertical pushing plates (Fig. 6) over a horizontal steel base on which the model is kept. Two of the oppositely facing plates (A and B of Fig. 6) are of fixed width while the other two (C and D) are telescopically collapsible. The rates of displacement of each pair of plates are the same in the case of pure constrictional deformation whereas in the case of general constriction the two rates are different. When the plates A and B move towards each other the widths of the plates C and D is reduced accordingly. The rate of movement of the plates can be controlled by changing the size of the pulley attached to the chain-gear system. The surface of the basal plate was lubricated with gear oil and the inner surfaces of the vertical plates were lubricated with liquid soap before placing the model in the machine.

For the single-layer experiments a circular sheet of modelling clay of 17 cm diameter and 1.5 or 2 mm thickness was sandwiched between two slabs of painter's putty each about 20 cm × 20 cm × 4 cm. The model materials were the same as those in the experiments of superposed buckling by Ghosh *et al.* (1992). For a model with a layer oblique to the principal axes, a block of painter's putty for the lower slab was first prepared and the required angle with the horizontal plane (the dip or apparent dip of the layer) was marked on the two opposite vertical walls. A stretched sitar wire was used to cut the slab along the marked lines. The circular sheet of modelling clay was placed on the inclined upper surface of this wedge of putty and the layer was then covered by the top slab of putty. The side walls of the model were trimmed. For multilayer models, modelling clay sheets of 1.5 or 2 mm thickness and of two different colours for alternate layers were prepared. The multilayer was built up by placing one sheet over another after greasing the interfaces to prepare a block of about 20 cm × 20 cm with a total thickness of 4–5 cm. The whole unit was then placed between two thick slabs of a mixture of modelling clay and painter's putty.

For all models in which the overburden above a folded layer could be removed the fold geometry could be directly studied. Some of the multilayered models were cut by a large number of horizontal sections at equal intervals. Photographs of the sections were taken with a constant focus of the camera and enlarged to the same magnification. Structure contour maps for selected interfaces were drawn from photographs. The fold geometry in the other models was reconstructed from close-spaced parallel vertical sections. In some of the rectangular models there was some edge effect near the contact with the driving plates. For such models the fold patterns in only the central parts of the models were considered.

EXPERIMENTAL RESULTS

Buckling of single layers under pure constriction

In the experiments described below the single embedded layer in a model was parallel to the horizontal $\lambda_2\lambda_3$-plane of pure constriction in which $\lambda_2 = \lambda_3 < 1$. When the horizontal shortening was small (about 10% in a radial direction) the competent layer was deformed to gentle domes and basins. Unlike the domes and basins produced in superposed buckling (Ghosh & Ramberg 1968, Skjernaa 1975, Ghosh *et al.* 1992), a constrictional deformation did not give rise to two distinct rows of domes or basins crossing each other. The plan view of the domes and basins were often irregular and, in some places, equant or slightly elongate. The elongate segments did not show any preferred orientation.

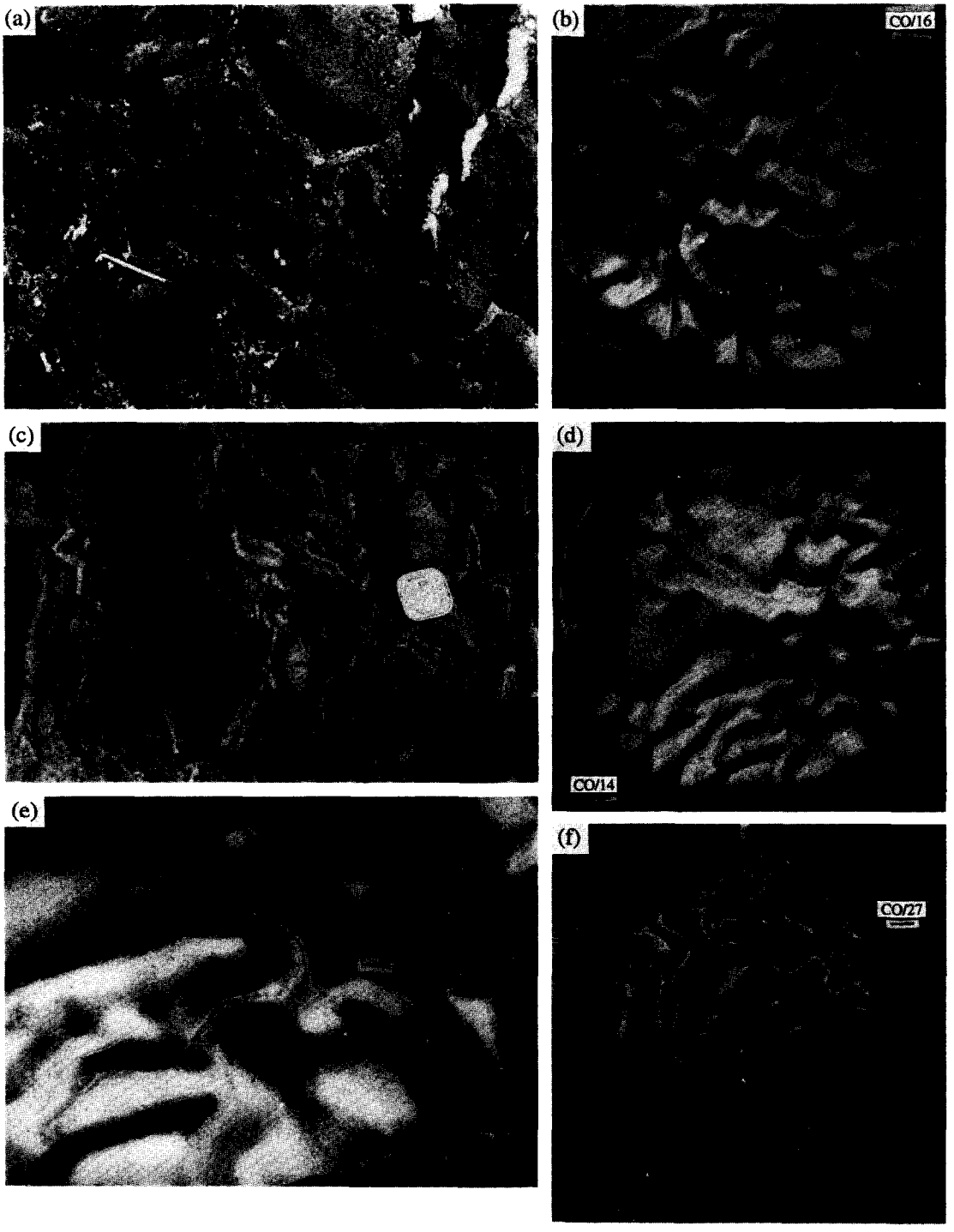

Fig. 2. (a) A late generation of domes and basins in close association with short segments of arcuate folds on subvertical bedding-parallel cleavage of garnet–quartz rock in the Aravalli schists from the Jharol area near Udaipur, India. Matchstick 4.5 cm in length. (b) Irregular domes and basins on a layer of modelling clay deformed by pure constriction. The overburden of putty has been removed. The bulk horizontal shortening in a radial direction is 18.8%. (c) Association of gentle domes and basins with arcuate folds. Madge's Corner, Kolar Schist Belt, S. India. Note the gentle fold with hair pin bends of the hinge line on the left central portion. Coin width—1.8 cm. (d) Association of domes and basins with short segments of arcuate folds in bulk pure constriction (horizontal shortening 17.7%). (e) Details of model shown in (d). Note the three-pronged spiral form in the central part. (f) Diversely oriented nonplane noncylindrical folds in association with a few remnants of domes and basins. The model was deformed by bulk pure constriction with horizontal shortening of 29.4%. Scale bar 1 cm in (b), (d) & (f). Scale bar 5 mm in (e).

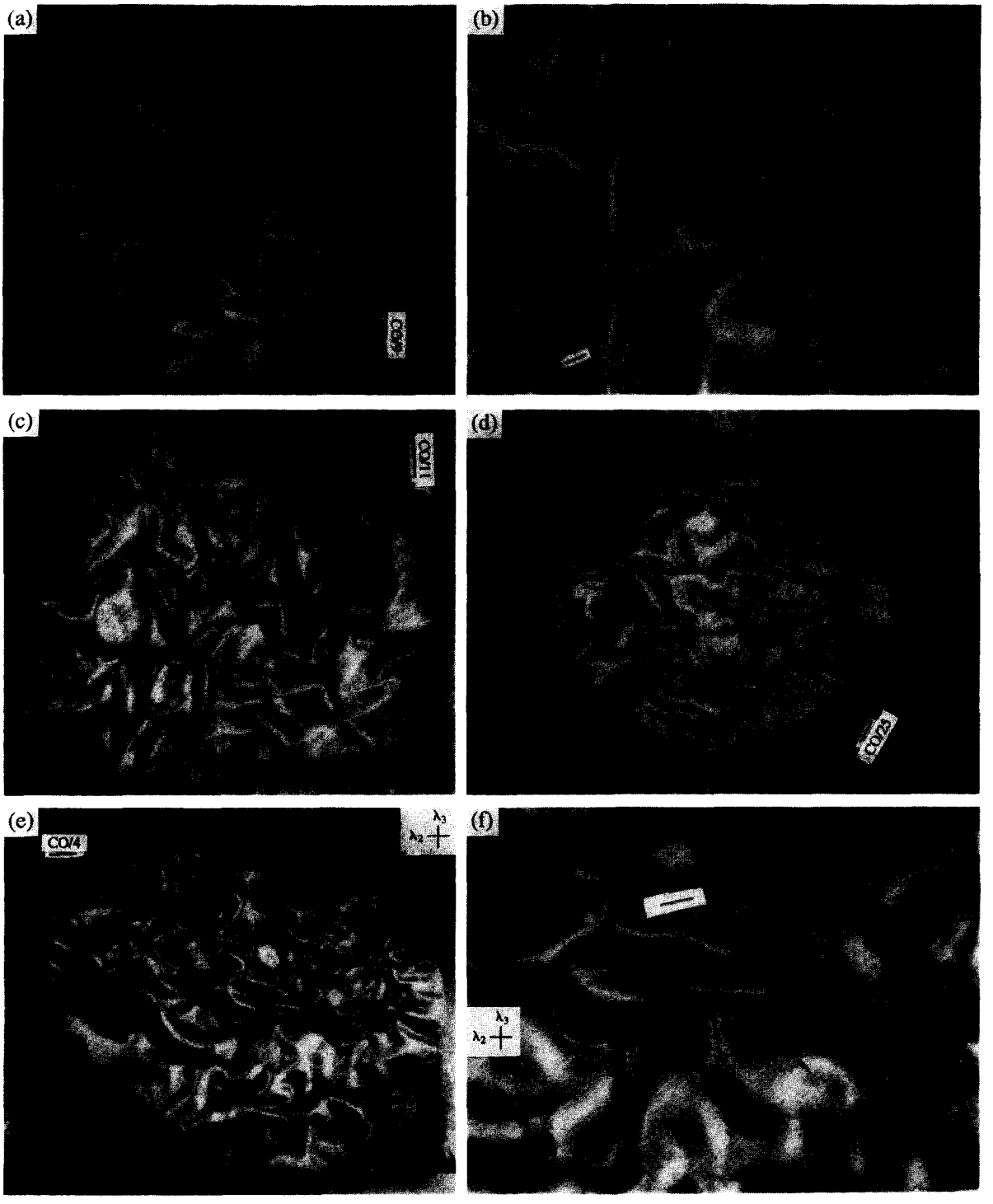

Fig. 3. (a) Characteristic fold interference in bulk pure constriction at moderately large deformation, with horizontal shortening of 28.8%. Note diversely oriented nonplane noncylindrical folds and joining up of differently oriented folds at domes or basins. (b) Details of model shown in (a). (c) Complex fold interference in bulk pure constriction at large horizontal shortening of 32.3%. (d) Fold interference produced by a general constrictional deformation, with the layer parallel to the $\lambda_2\lambda_3$ plane. $\lambda_2 = 0.58$, $\lambda_3 = 0.46$. (e) Fold interference produced by a general constrictional deformation, with the layer parallel to the $\lambda_2\lambda_3$ plane. $\lambda_2 = 0.63$, $\lambda_3 = 0.53$. (f) Details of model shown in (e). Scale bar 1 cm in (a), (c), (d) & (e). Scale bar 5 mm in (b) & (f).

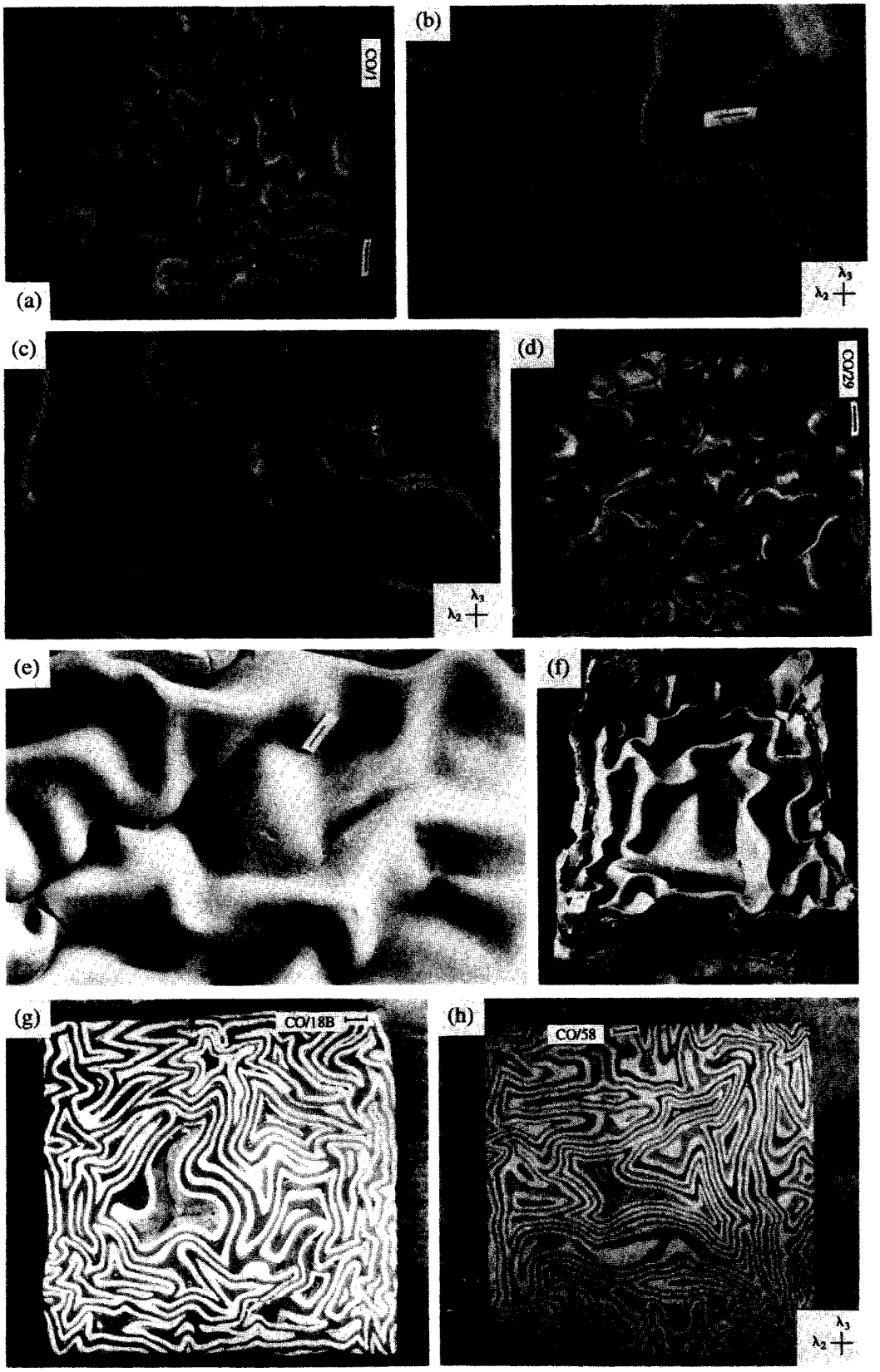

Fig. 4. (a) Fold interference produced in general constriction. Note the dominant fold trend perpendicular to λ_3, a less dominant trend parallel to λ_3 and the occurrence of a few domes and basins, $\lambda_2 = 0.68$, $\lambda_3 = 0.50$. (b) & (c) Details of model shown in (a). Note the occurrence of two sets of nearly orthogonal folds which link up in smooth arcs. (d) Fold interference produced in general constriction $\lambda_2 = 0.58$, $\lambda_3 = 0.38$. (e) Association of domes and basins with folds with curvilinear hinges in a model deformed by general constriction. $\lambda_2 = 0.7$, $\lambda_3 = 0.46$. (f) Interfering folds produced in a multilayer under bulk pure constriction. The upper part of the multilayer has been removed to expose the folds in a central layer, $\lambda_2 = \lambda_3 = 0.42$. (g) Horizontal section through multilayer model deformed by bulk pure constriction. $\lambda_2 = \lambda_3 = 0.42$. Note spiral form of the outcrop in the centre and amoeboid outcrop near the top. (h) Horizontal section through a multilayer model under bulk pure constriction. $\lambda_2 = \lambda_3 = 0.49$. Note the triangular outcrops of interfering chevron folds. Scale bar 1 cm in (a), (d), (f), (g) & (h). Scale bar 5 mm in (b), (c) & (e).

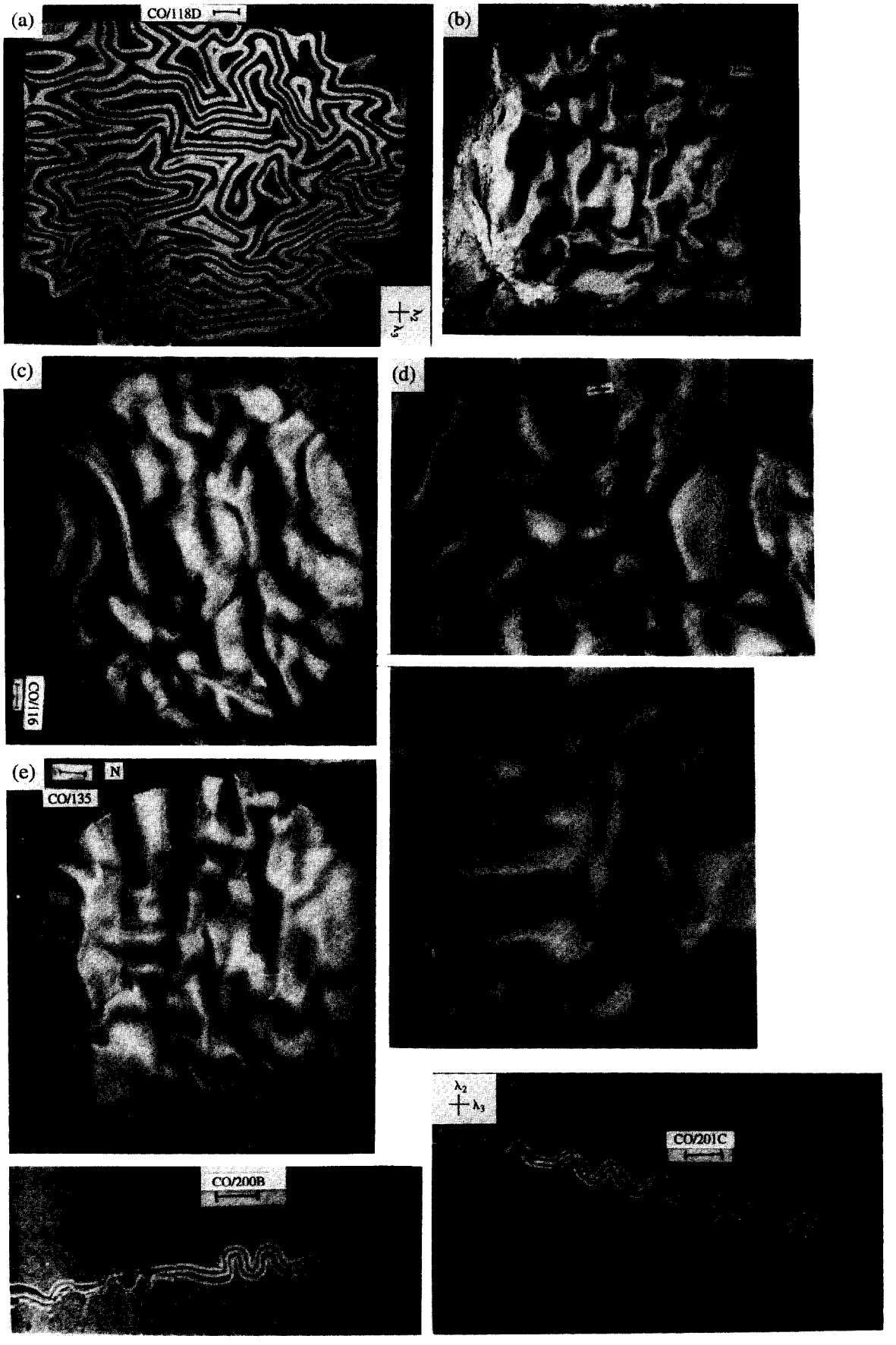
(a)
CO/118D
(b)
(c)
CO/119
(d)
(e)
N
CO/135
CO/200B
CO/201C

When the equal horizontal shortening was somewhat larger (about 15–20%), the fold pattern became more complex (Figs. 2b & d) by progressive replacement of the dome-and-basin structure by diversely oriented curvilinear fold trends. Figures 2(d) & (e) show a model with an all-sided horizontal bulk shortening of 17.7%, i.e. with $\lambda_2 = \lambda_3 = 0.68$. In this model the domes and basins are closely associated with short segments of folds in which a distinct hinge line is discernible. These linear arcuate fold-trends do not have any preferred orientation. The fold geometry suggests that replacement of the initial dome-and-basin pattern starts by nucleation of short arcuate folds along the borders of the domes or basins; with progressive deformation the meandering fold-trends coalesce with each other around an irregular dome or a basin. The arcuate folds propagating lengthwise encroach from different sides on the flanks of the domes and basins so that their areas are greatly reduced and the boundary of an isolated dome or basin becomes serrated or acquires a three-pronged or multipronged amoeboid appearance (Fig. 2e).

When the shortening along λ_2 or λ_3 is moderately large (>20%), folds with distinct and curved hinge lines gain prominence over a dome-and-basin structure (Figs. 2f and 3a & b). The segments of diversely oriented sinuous folds link up with one another and their close juxtaposition with the remnants of domes and basins gives rise to a very complex fold geometry (Fig. 3c).

A remarkable feature of the present series of experiments is that the gentle domes and basins which develop in the initial stage of constrictional deformation do not retain the dome-and-basin structure with progressive shortening. The domes and basins never evolve into tubular or sheath-like folds. Where a domal or basinal structure is retained in isolated domains, an increase in amplitude is accompanied by development of smaller folds on the flanks which gives the outcrop pattern an amoeboid or star-like appearance (Figs. 2e and 7). In the major part of these models, however, a large constrictional deformation causes a replacement of the dome-and-basin structure by tight folds with strongly sinuous hinge lines. The folds show various patterns or arcuation, virgation and linkage (Bucher 1933). Some of these characteristic patterns are shown in Fig. 8.

The initial stage of replacement of a dome-and-basin structure by curvilinear fold hinges produces both weakly sinuous hinge lines and some hinge lines with hairpin bends. The folds with hairpin bends may be open or may show a moderate tightness; it is likely that they are mostly produced by merging together of differently oriented separate fold-arcs that were propagating lengthwise and were at a low angle to each other. The structure is very similar to the natural example shown in Fig. 2(c). Once the dome-and-basin structure is largely replaced by curvilinear folds, further constriction causes a tightening of the individual folds, and there is at the same time an increase in the curvatures of the hinge lines and axial surfaces of these folds. The final curvatures of the hinge lines are therefore largely a result of linking up of fold arcs and are partly a result of accentuation of initial curvatures during progressive deformation.

There is a problem of nomenclature for the description of the fold geometry produced in a single-phase constrictional deformation. The folds with sinuous hinge lines are nonplane noncylindrical folds. Since the development of the folds and the curving of the hinge lines and axial surfaces are broadly contemporaneous, the fold geometry cannot be described in terms of F_1 and F_2. The main folds with sinuous hinge lines will be described here as F with axial surface S. The folds which develop due to curving of the hinge line and the axial surface of F will be described as f (Fig. 9) with axial surface s.

The hinge lines of F, in spite of diverse orientations, remain close to the overall orientation of the layer which is here parallel to the $\lambda_2\lambda_3$-plane of bulk strain. There is only a small range of variation of the plunge of F, and the folds remain essentially horizontal in most places (with plunge varying between 0 and 10°). Larger values of plunge of F are rarely encountered near the fold terminations. The attitudes of the F-fold hinges were measured in some of the models. The measurements were made at more or less equal intervals as far as practicable. The trend of the hinge line was directly measured with a clinometer compass. To measure the plunge a specially made small and light clinometer was used. The plunge reading was correct to ±2°. Equal-area projection of the hinge lines shows that, as expected, the axes of F occur along a peripheral girdle (Fig. 10a). The diversely oriented axial surfaces (S) of the F folds are essentially vertical (i.e. normal to the enveloping surface) and are expected to give a vertical β_s. The axial surfaces (s) of f are also subvertical and there is no preferred orientation of their strike lines. The symmetry of fabric as a whole is axial, with the axis of symmetry parallel to the axis of

Fig. 5. (a) Horizontal section through multilayer model deformed by general constriction with $\lambda_2 = 0.75$ and $\lambda_3 = 0.51$. Note the occurrence of both crescentic and hook-shaped outcrops, with the crescents oriented in different directions. (b) Fold interference in a layer initially inclined at 10° to the $\lambda_2\lambda_3$ plane. The model was deformed by bulk pure constriction, with $\lambda_2 = \lambda_3 = 0.65$. Note that the dominant fold axis is in the down dip direction (top to bottom). The fold interference pattern is similar to that of models deformed by layer-parallel general constriction, (c) Inclined layer deformed by bulk general constriction. The layer is inclined towards the bottom of the figure. λ_3 is parallel to the strike of the layer (left to right). The layer had an initial dip of 15° and final dip of 27°. $\lambda_2 = 0.64$, $\lambda_3 = 0.60$. (d) Details of model shown in (c). (e) Layer-normal view of model with inclined layer. The dip of the layer is roughly towards the lower right corner. The two dominant sets of folds are parallel to R_1 and R_2. The initial strike of the layer is 45° with respect to λ_3 and the initial dip is 10° with respect to the $\lambda_2\lambda_3$-plane. (f) Details of the model shown in (e). Note the absence of a consistent overprinting relation between the fold sets. (g) Horizontal section through model showing thin multilayer parallel to vertical λ_1 axis. The model was deformed by pure constriction. $\lambda_2 = \lambda_3 = 0.55$. (h) Horizontal section through a model showing thin multilayer parallel to vertical λ_1 axis. The layering was initially at an angle of 10° to the direction of λ_3. $\lambda_2 = 0.69$, $\lambda_3 = 0.40$. Note the development of tight asymmetrical folds with planar axial surfaces in the central part. Scale bar 1 cm in (a), (b), (c), (e), (g) & (h). Scale bar 5 mm in (d) & (f).

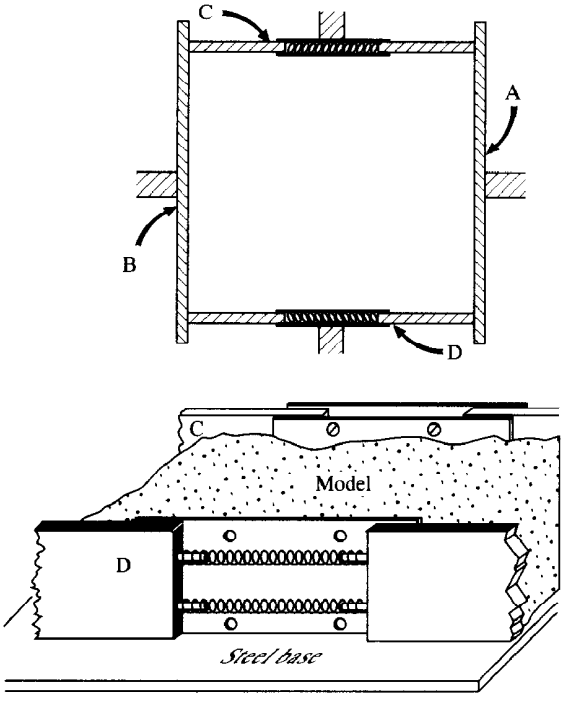

Fig. 6. Diagrammatic sketch of plan and side views of the driving plates of the apparatus.

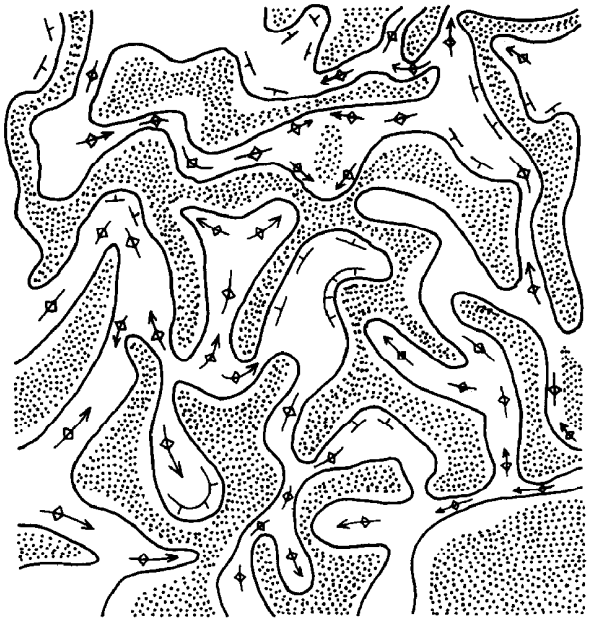

Fig. 7. Plan view of a part of a model (CO/11) showing the antiformal (blank) and synformal (stippled) areas. The model was deformed by layer-parallel pure constriction. Note the amoeboid appearance of the synformal structure in the central part produced by joining up of diversely oriented folds.

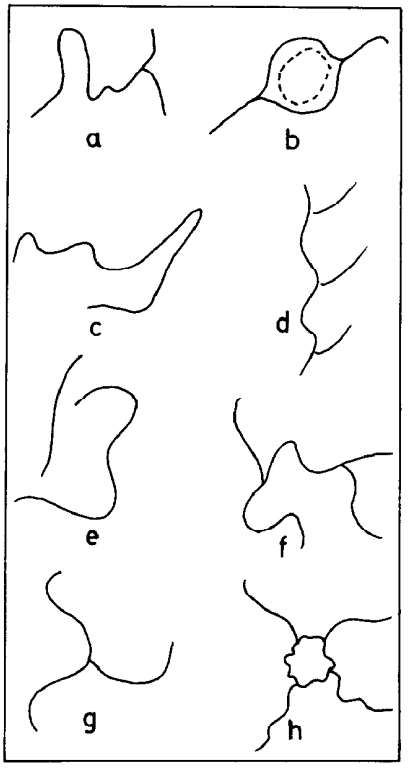

Fig. 8. Patterns of fold hinge arcuations and linkages produced in models deformed by pure constriction. In (b) the bold lines are antiformal hinge lines and the area surrounded by the dashed lines is a basin. In (h) the central region is a domal structure; diversely oriented folds with sinuous hinge lines terminate against it.

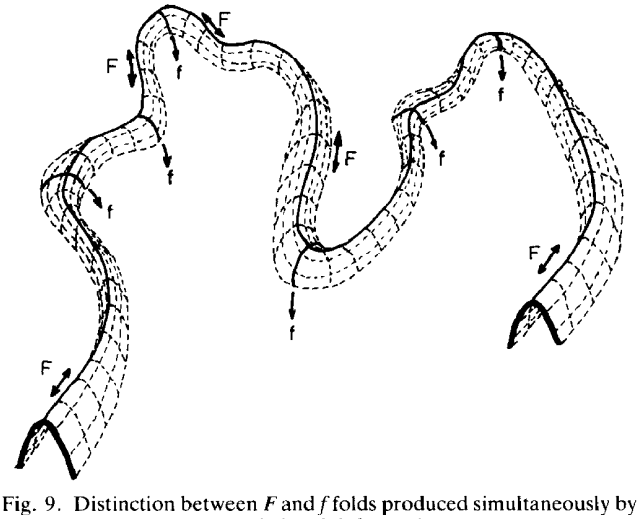

Fig. 9. Distinction between *F* and *f* folds produced simultaneously by a constrictional deformation.

revolution of the prolate ellipsoid for bulk constrictional deformation.

Buckling of single-layers under general constrictional deformation

Buckling folding under a general constrictional deformation (Figs. 3d–f and 4a, d & e) produces a close association of domes and basins with folds having long sinuous hinge lines (*F* folds). Unlike the case of pure constriction, the *F* folds appear even in an early stage of deformation. With progressive deformation the areas of domes and basins are reduced and the continuity of the *F* folds increases. Although the associated domes and basins often have irregular outlines, they are mostly elongate. It is suggested that with progressive deformation the segments of elongate domes and basins are tightened across their length, propagate lengthwise and link up with other segments to produce the *F* folds with

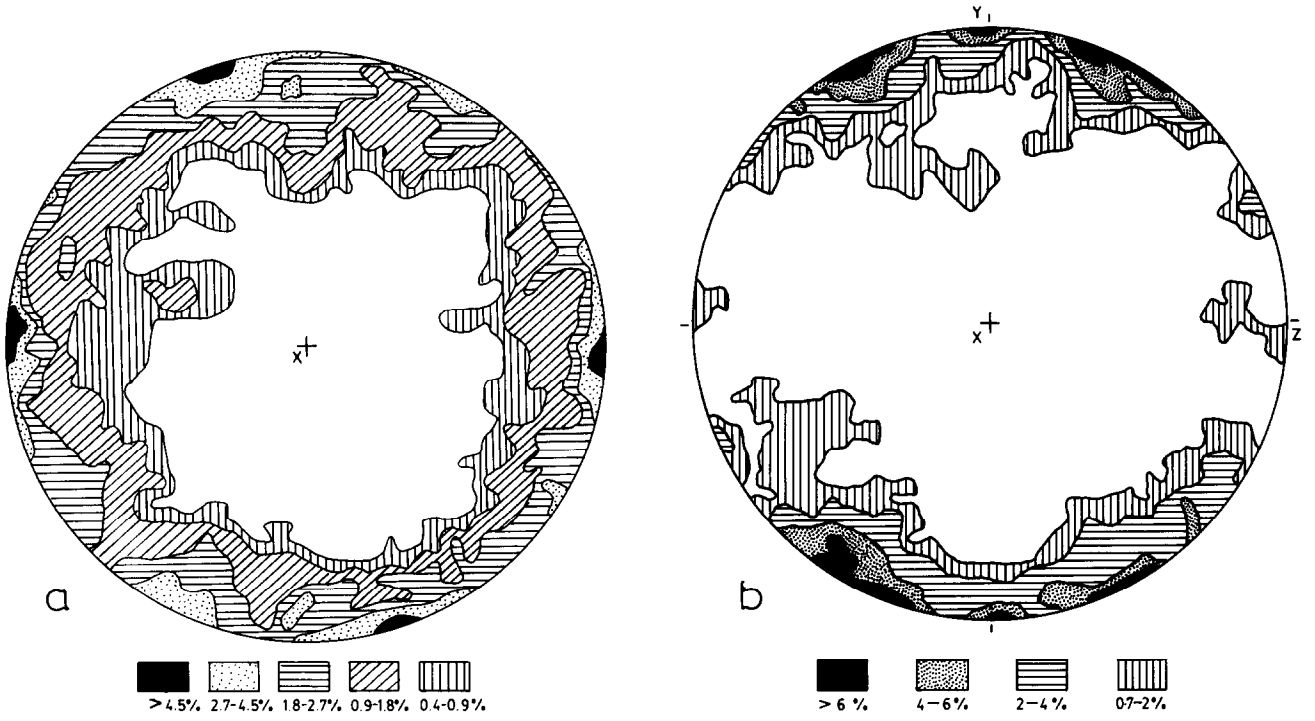

Fig. 10. Lower hemisphere equal-area projection of hinge lines of F folds in models deformed by constrictional deformation for (a) 220 measurements of a model deformed by pure constriction with $\lambda_2 = \lambda_3 = 0.51$, and for (b) 250 measurements of a model deformed by general constriction with $\lambda_2 = 0.58$, $\lambda_3 = 0.38$. Contour values given in percent per 1% of area.

sinuous hinge lines. However, a few remnants of domes and basins may be retained even when the deformation is large (Figs. 4c & d).

Figure 10(b) shows the equal-area projection of the F fold hinges of a model. Evidently, the interference pattern of buckling folds produced under a general constrictional deformation is not as unsystematic as in pure constriction. The overall trend of the hinge lines and the axial surfaces of many of the curvilinear F folds are perpendicular to the λ_3 direction (Figs. 3d & e). The f folds produced by the curving of the axial surfaces of the F folds often have axial surfaces sub-parallel to the λ_3-direction (Fig. 3d). Although most of the F folds are weakly arcuate, these are associated with some folds with hinge lines curved to a hair pin bend (e.g. Figs. 3f, 4a & d). These must have been produced by the joining up of F folds which curve at a low angle to each other. In some of the models there are two distinct overall trends of the sinuous F fold hinges, a dominant one sub-parallel to the λ_2-axis and a less dominant one sub-parallel to the λ_3 (Figs. 3f and 4b & c). Unlike the fold systems in superposed deformation, the two directions of folds do not show overprinting relations but join up in smooth arcs of right angular bends. The overall trends of the folds produced in a general constrictional deformation are not all sub-parallel to λ_3 and λ_2 directions; there are often a relatively smaller number of arcuate fold segments which are oblique to the principal axes of bulk strain (e.g. Fig. 4d). The axial surfaces of the F-folds are often deformed to asymmetric shapes.

The fold interference pattern produced in a general constrictional deformation may resemble in certain domains the interference pattern produced by superposed deformations. Where there is a preponderance of F-folds with the average trend sub-parallel to the λ_2-axis, and with the axial surfaces of the corresponding f folds sub-parallel to λ_3, the structure is morphologically indistinguishable from the Type 2 interference pattern of fold superposition. However, if we consider a larger domain in which there is a linking up of different folds or an association of curvilinear fold hinges with domes and basins, the pattern can be distinguished as a product of interference of broadly synchronous folds resulting from constrictional deformation.

Buckle folding in multilayers in constrictional deformation

The geometry of fold interference in the multilayered models was similar to that of single layers. However, the type of multilayers used in these experiments was such that conjugate and chevron folds were dominant. In bulk pure constriction the deformed models often showed domal and basinal structures with more or less flat segments and steep flanks. These are surrounded by sinuous trends of chevron folds (Fig. 4f). As in single-layer fold-interference under layer-parallel pure constriction, the axial surfaces of the F and f folds are diversely oriented. Domal or basinal structures have often been produced by the abutting of a sharp-hinged F fold against another or by the joining of three or more folds. These structures have given rise to triangular (Fig. 4h), star-shaped and amoeboid outcrops the arms of

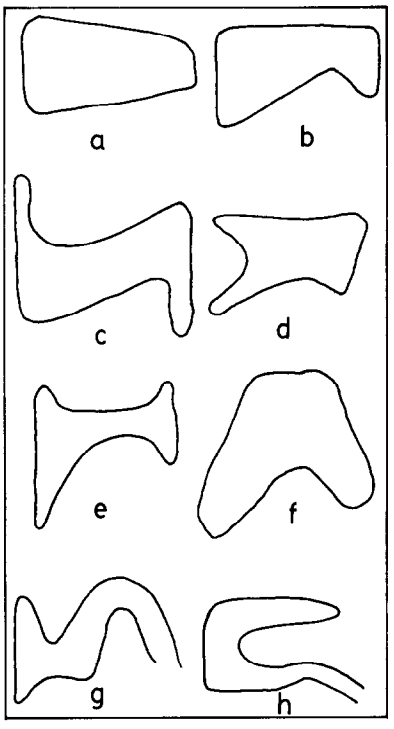

Fig. 11. Some characteristic outcrop patterns (sections normal to λ_1) produced by pure constrictional deformation of multilayer models.

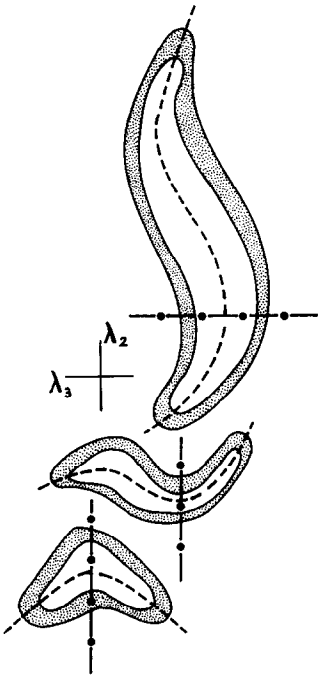

Fig. 12. Schematic diagram showing occurrence of differently oriented crescentic outcrops in layered models deformed in a general constrictional deformation. The crescents show diversely oriented axial surface traces of *F* folds (dashed lines) and of *f* folds (dot-and-dash lines). Since the *f* axial traces of some of the crescents are at right angles to those of others, the structure may give the erroneous impression that an early set of nonplane noncylindrical folds produced by two deformations has been reoriented by a third deformation.

which sometimes swerve in the same sense to produce a spiral form (Fig. 4g). Such outcrop patterns produced by the joining up of differently oriented fold-trends are quite distinct from the oval, crescentic and hook-shaped outcrops characteristic of superposed folds. Although the latter types of outcrop patterns were also produced in the multilayers, their shapes are often greatly modified by the differently oriented conjugate and chevron folds (Fig. 11).

As in the case of single-layer folds, for a general constrictional deformation, with the layering of the multilayered models parallel to the $\lambda_2\lambda_3$ plane, the dominant *F* folds have sinuous or zig-zag axial surfaces and have a generalized fold trend more or less perpendicular to the λ_3 axis; the corresponding *f* folds have axial surfaces sub-parallel to λ_3. However, the *F* folds are not all at a right angle to λ_3 and there are relatively short segments of *F* with gently curved hinge lines which are more or less parallel to λ_3 and with the axes and axial surfaces of the corresponding *f* folds at a high angle to the trend of *F* folds. Because of the dominance of two orthogonal fold trends, *F* and *f*, the interference pattern can not be easily distinguished in small isolated domains from the patterns produced in two successive deformations. Over a relatively larger domain, however, the fold interference pattern cannot be explained by superposition of two separate deformations. Thus, for example, the *f*-fold axial traces of crescentic and hook-shaped fold closures on horizontal sections of the models are oriented parallel to both λ_2 and λ_3 directions (Figs 5a and 12). The geometrical relations do not indicate that between the two orthogonal sets of *F* or between the two sets of *f* folds, one set is earlier than the other.

Layers oblique to the $\lambda_2\lambda_3$ plane

We do not obtain an unsystematic pattern of fold orientations in layers oblique to the $\lambda_2\lambda_3$ plane in either a pure or a general constriction. If the layer initially makes a small angle ($<10°$) to the $\lambda_2\lambda_3$ plane of *pure constriction* and the deformation is small, the interference pattern shows an association of equant and slightly elongate domes and basins with sinuous borders. However, if the deformation is moderately large, the angle between the enveloping surface and the $\lambda_2\lambda_3$ plane increases, and the folds, in spite of the sinuosity of the hinge lines and the presence of domains of domes and basins, have a preferred orientation of the generalized hinge lines down the dip of the layer (Fig. 5b). More or less similar patterns are obtained in low-dipping (10°–15°) layers (Figs. 5c & d) deformed in a bulk general constriction; however, the generalized direction of the dominant hinge lines is not necessarily down the dip of the enveloping surface. The models show a dominant trend of arcuate folds parallel to the major axis of the sectional strain ellipse. These folds are sometimes associated with short segments of folds at a right angle to the dominant trend. The two fold trends may link up in a smooth arc (Figs. 5e & f). They generally do not show consistent overprinting relations. Along with this dominant pattern, the models usually have certain domains in which well-defined *F* folds and the domes and basins link up to form complex fold patterns. Such patterns obtained by linking up of curvilinear hinge lines and of domes and basins are characteristic of constrictional deformation

and are not found in experiments of superposed buckling (Ghosh & Ramberg 1968, Skjernaa 1975, Ghosh *et al.* 1992, 1993, Grujic 1993).

DISCUSSION

The experiments indicate that interfering fold patterns produced in a constrictional deformation are not always unsystematic. A pattern of irregular domes and basins may indeed develop if the deformation is small and there is more or less equal contraction in all directions in the plane of the layer. With an increase in deformation this dome-and-basin pattern is progressively replaced by diversely oriented sinuous fold hinges with an overall axial symmetry of the different orientations of F and f fold axes and axial surfaces. A pure constrictional deformation with $\lambda_2 = \lambda_3$ is, however, likely to be rare in nature. Even in a pure constrictional bulk deformation, the principal contractions in the plane of the layering are equal only if the layering remains parallel to the $\lambda_2\lambda_3$ plane during the entire course of deformation. The pattern of fold interference is not unsystematic when the principal layer-parallel contractions are unequal. The F folds are then mostly nonplane noncylindrical and there are, in general, two orthogonal fold trends of both F and f parallel to R_1 and R_2 (the principal axes of the strain ellipse on the plane of the layer). An important result of the present series of experiments is that the fold interference patterns produced by unequal layer-parallel contractions often resemble the Type 2 interference pattern of superposed folding. The interference pattern produced by constrictional deformation can be distinguished in many cases by (i) close association of nonplane noncylindrical folds with domes and basins, (ii) strongly arcuate hinge lines of more or less open folds, (iii) characteristic outcrop patterns resulting from the meeting of three or more differently oriented F folds and (iv) absence of a consistent overprinting relation between F (or f) folds of different orientations. Yet a distinction, especially in relatively small domains, may not always be possible from the fold geometry alone. This may be one of the reasons why bulk constrictional deformation has so rarely been identified in the field.

In a layer oblique to the principal axes of bulk constrictional deformation, the ratio of the rates of layer-parallel instantaneous contractions along the principal directions (R_1 and R_2) in the plane of the layer changes in the course of progressive deformation (e.g. Ramberg & Ghosh 1977, Treagus & Treagus 1981). Depending on the initial orientation of the layer and on the nature of deformation, the buckling folds on an oblique layer may show different evolutionary patterns. A layer may undergo unequal layer-parallel contractions along R_1 and R_2 throughout the entire period of deformation (curves restricted to field 3 of Fig. 13; cf. Ramsay & Huber 1983, fig. 4.10). It may, after a certain period of layer-parallel constriction, attain an orientation in which the long axis R_1 of the sectional strain ellipse becomes a

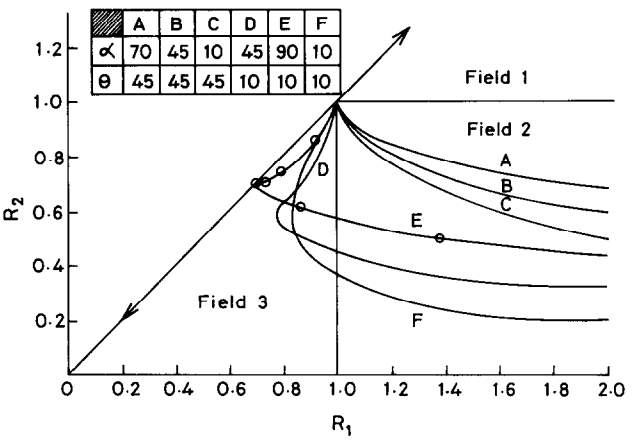

Fig. 13. Plot of semi-axes of sectional strain ellipse, R_1 against R_2, showing three separate fields. Field 3 of bulk constrictional deformation is for sectional strain ellipses in which R_1 and R_2 are both <1. Curves A–F show progressive changes in R_1 and R_2 on oblique layers of different orientations for $k' = [\ln(X/Y)/\ln(Y/Z)] = 4$. (cf. Ramsay & Huber 1983 fig. 4.10). The six circle marks on the curve E correspond to the strain ellipses of Fig. 14. α = Initial angle between λ_3 axis and line of intersection of the inclined plane with the $\lambda_2\lambda_3$ plane. θ = Initial angle of the plane with the $\lambda_2\lambda_3$ plane.

direction of instantaneous extension. The earlier interference pattern characteristic of a general constriction, may, subsequently become partially masked by the development of a single direction of folding parallel to the R_1 axis (e.g. curves D, E and F of Fig. 13). Layers which are initially steep or moderately steep with respect to the $\lambda_2\lambda_3$-plane will, under a pure or general bulk constriction (curves restricted to field 2 of Fig. 13), develop only a single direction of folding. We may even have the case in which the aspect ratio of the constrictional strain ellipse gradually decreases until there is a transient phase of layer-parallel pure constriction with $R_1 = R_2 < 1$, and then increases once again with a switching of the positions (Fig. 14) of R_1 and R_2 axes (curve E of Fig. 13). Although there will be a layer-parallel constriction in both the earlier and later phases of deformation of the layer, the dominant F folds in the later phase of deformation will be perpendicular to the dominant F folds of the earlier phase. The structure may then resemble that formed by superposed deformations.

It has been suggested that cylindrical polyclinal folds may develop by stretching parallel to the fold axis and a shortening in all directions normal to it (Sander 1948, referred to by Turner & Weiss 1963, p. 506). The structure was described as *Schlingen* (see also Fairbairn 1949, pp. 181–182). The present series of experiments indicates that layers parallel to or at a low angle to the λ_1-axis of pure or general constrictional deformation may give rise to a set of cylindrical folds subparallel to the direction of maximum stretching. However, the folds in transverse profile may not be polyclinal in either pure (Fig. 5g) or general (Fig. 5h) constrictional deformation. In a general constrictional deformation, with the layer subparallel to the λ_1-axis and at an acute angle to the λ_3-axis, the folds produced in a multilayer are asymmetrical (Fig. 5h), with the average orientation of the axial surfaces approximately parallel to the

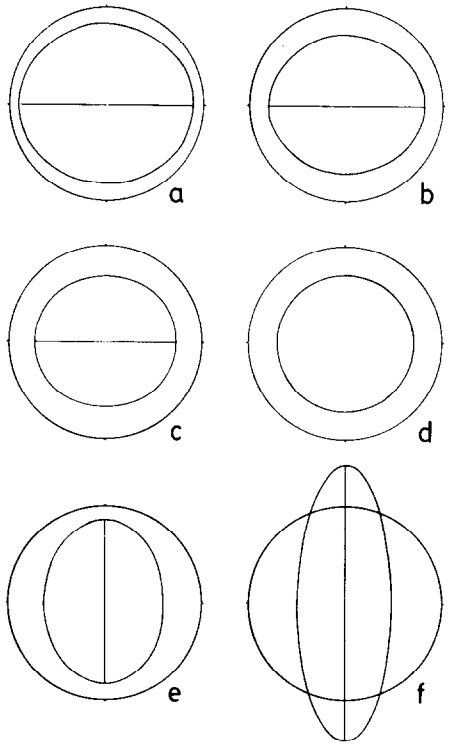

Fig. 14. The orientations of sectional strain ellipses at successive stages, on a layer which was parallel to the Y axis of bulk strain and was initially dipping at an angle of 10° to the YZ-plane (curve E of Fig. 13). The bulk deformation is a general constriction with $k' = 4$. For each stage the horizontal Y axis is from left to right and the direction from top to bottom is down-dip. In the initial stages (a), (b) & (c) there is a shortening along both the principal directions, the long axis of the strain ellipse being parallel to Y. At stage (d) the sectional strain ellipse is a circle of radius less than unity. Beyond this stage of progressive deformation the long axis of the sectional strain ellipse points down-dip. At stage (f) and beyond, the down-dip direction becomes a direction of finite extension. The successive stages of bulk deformation are (a) $\lambda_1 = 1.82$, $\lambda_2 = 0.82$, $\lambda_3 = 0.67$, (b) $\lambda_1 = 3.32$, $\lambda_2 = 0.67$, $\lambda_3 = 0.45$, (c) $\lambda_1 = 6.05$, $\lambda_2 = 0.55$, $\lambda_3 = 0.30$, (d) $\lambda_1 = 11.02$, $\lambda_2 = 0.45$, $\lambda_3 = 0.20$, (e) $\lambda_1 = 20.08$, $\lambda_2 = 0.37$, $\lambda_3 = 0.13$, (f) $\lambda_1 = 66.69$, $\lambda_2 = 0.24$, $\lambda_3 = 0.06$.

$\lambda_1\lambda_2$-plane. With the constrictional apparatus used for this series of experiments, the contractions in the λ_2 or λ_3 direction could not be made very large. It is however reasonable to suggest that for a very large constrictional deformation the axial surfaces of the tightened F folds would again be folded and give rise to a set of coaxial folds, i.e. a set of nonplane cylindrical folds (Fig. 15). Indeed, in this theoretical model, repeated development of coaxial folds may also be possible. If the bulk deformation is a general constriction, with $\lambda_2 > \lambda_3$, the axial surfaces of the successive generations of folds are likely to be perpendicular to one another.

Interfering folds produced in constrictional deformations can be analyzed and distinguished with a greater confidence if the orientations and the time of formation of cleavages and lineations are studied along with the fold geometry. Treagus & Treagus (1981) pointed out that a single cleavage will develop parallel to the XY-plane of the bulk strain ellipsoid and transecting the arcuate hinge lines and the curved axial surfaces of the folds. In addition, as these authors also noted, with progressive tightening of the folds and with the limbs coming closer together, a cleavage sub-parallel to the

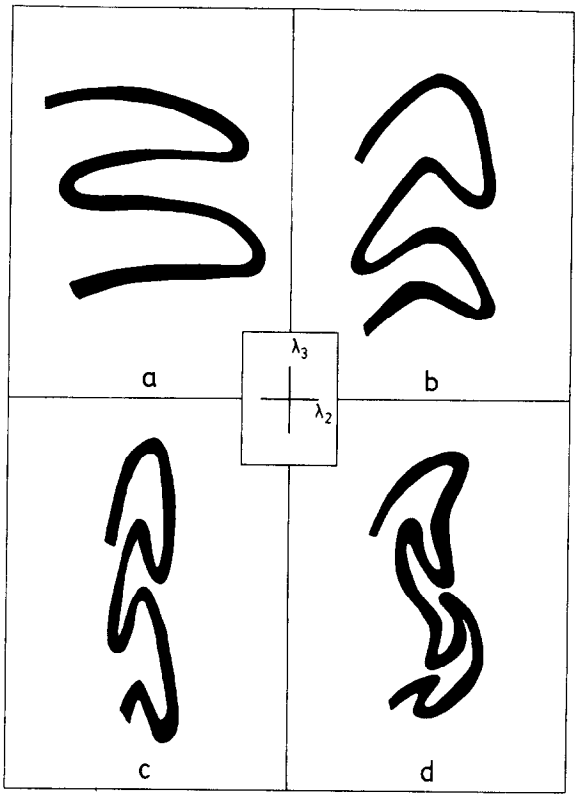

Fig. 15. Suggested model of development of coaxial folds in a bulk constrictional deformation, with $\lambda_2 > \lambda_3$.

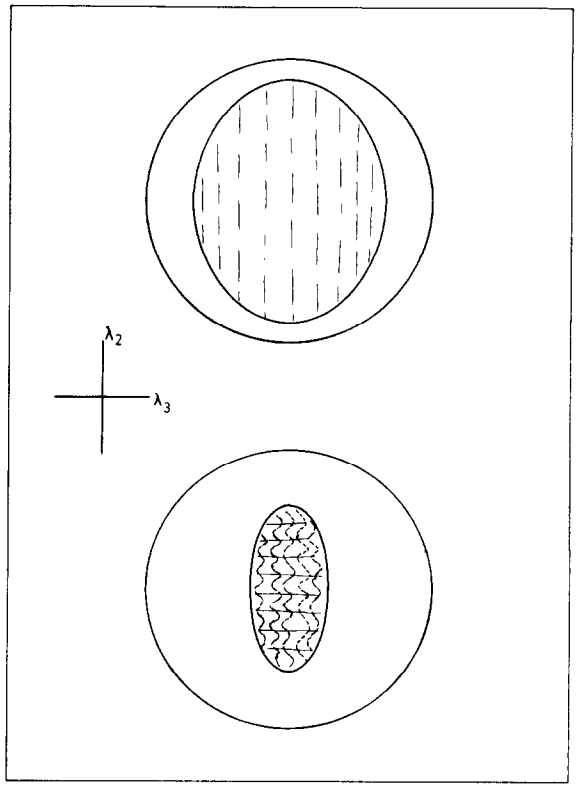

Fig. 16. Suggested model of development of a cleavage and crenulation cleavage in the same continuous deformation in general constriction.

hinge line may develop in the competent layers. Nevertheless, it is conceivable that a single-phase constrictional deformation may give rise to more than one cleavage. Once a cleavage develops parallel to the $\lambda_1\lambda_2$-plane of the bulk strain ellipsoid of a general constrictional deformation, it creates a mechanical anisotropy in the rock. With continued shortening parallel to the direction of λ_2, this cleavage will be crenulated, with axes parallel to λ_1 and with axial surfaces parallel to the $\lambda_1\lambda_3$-plane (Fig. 16). If the total shortening along the intermediate axis of strain is sufficiently large, a crenulation cleavage may develop perpendicular to the main cleavage in the course of a single-phase constrictional deformation.

Acknowledgements—This work was supported by the Council of Scientific and Industrial Research, India. The authors are grateful for the constructive criticisms by Lilian Skjernaa, Peter Hudleston and an anonymous reviewer.

REFERENCES

Bucher, W. H. 1933. *The Deformation of the Earth's Crust*. Princeton University Press.

Fairbairn, H. W. 1949. *Structural Petrology of Deformed Rocks*. Addison-Wesley Publishing Company.

Flinn, D. 1962. On folding during three-dimensional progressive deformation. *J. geol. Soc. Lond.* **118**, 385–433.

Ghosh, S. K. 1993. *Structural Geology: Fundamentals and Modern Developments*. Pergamon Press.

Ghosh, S. K. & Ramberg, H. 1968. Buckling experiments on intersecting fold patterns. *Tectonophysics* **5**, 89–105.

Ghosh, S. K. & Sengupta, S. 1985. Superposed folding and shearing in the Western quartzite of Kolar Gold Field. *J. Indian Soc. Earth Sci.* **12**, 1–8.

Ghosh, S. K., Mandal, N., Khan, D. & Deb, S. 1992. Modes of superposed buckling in single layers controlled by initial tightness of early folds. *J. Struct. Geol.* **14**, 381–394.

Ghosh, S. K., Mandal, N., Sengupta, S., Deb, S. K. & Khan, D. 1993. Superposed buckling in multilayers. *J. Struct. Geol.* **15**, 95–111.

Grujic, D. 1993. The influence of initial fold geometry on Type 1 and Type 2 interference patterns: an experimental approach. *J. Struct. Geol.* **15**, 293–307.

Hobbs, B. E., Means, W. D. & Williams, P. F. 1976. *An Outline of Structural Geology*. John Wiley & Sons.

Ramberg, H. 1959. Evolution of ptygmatic folding. *Norsk. geol. Tiddskr.* **39**, 99–151.

Ramberg, H. 1966. The Scandinavian Caledonides as studied by centrifuged dynamic models. *Bull. geol. Inst. Univ. Upsala* **43**, 1–72.

Ramberg, H. & Ghosh, S. K. 1977. Rotation and strain of linear and planar structures in three-dimensional progressive deformation. *Tectonophysics* **40**, 309–337.

Ramsay, J. G. 1967. *Folding and Fracturing of Rocks*. McGraw-Hill, New York.

Ramsay, J. G. & Huber, M. I. 1983. *The Techniques of Modern Structural Geology*. 1. *Strain analysis*. Academic Press, London.

Ramsay, J. G. & Huber, M. I. 1987. *The Techniques of Modern Structural Geology*. 2. *Folds and fractures*. Academic Press, London.

Ramsay, D. M. & Sturt, B. A. 1973a. An analysis of noncylindrical and incongruous fold pattern from the Eo-Cambrian rocks of Söröy, northern Norway. I. Noncylindrical, incongruous and aberrant folding, *Tectonophysics* **18**, 81–107.

Ramsay, D. M. & Sturt, B. A. 1973b. An analysis of noncylindrical and incongruous fold pattern from the Eo-Cambrian rocks of Söröy, northern Norway. II. The significance of synfold stretching lineation in the evolution of noncylindrical folds. *Tectonophysics* **18**, 109–121.

Roberts, J. L. 1959. Fold structures in Dalradian rocks of Knapadale, Argyllshire. *Geol. Mag.* **96**, 221–229.

Skjernaa, L. 1975. Experiments of superimposed buckle folding. *Tectonophysics* **27**, 255–270.

Stringer, P. & Treagus, J. E. 1980. Non-axial planar S_1 cleavage in the Hawick rocks of the Galloway area, Southern Uplands, Scotland. *J. Struct. Geol.* **2**, 317–331.

Treagus, J. E. & Treagus, S. H. 1981. Folds and strain ellipsoid. *J. Struct. Geol.* **3**, 1–17.

Turner, F. J. & Weiss, L. E. 1963. *Structural Analysis of Metamorphic Tectonites*. McGraw-Hill Book Co.

Weiss, L. E. 1959. Structural analysis of the basement system at Turoka, Kenya. *Overseas Geology and Mineral Resources* **7**, 3–35, 123–153.